$\mathcal{PT}$-symmetric coupler with $\chi^{(2)}$ nonlinearity

K. Li,[1] D. A. Zezyulin,[2] P. G. Kevrekidis,[1] V. V. Konotop,[2] and F. Kh. Abdullaev[3,4]

[1]*Department of Mathematics and Statistics, University of Massachusetts, Amherst, Massachusetts 01003-4515, USA*

[2]*Centro de Física Teórica e Computacional, and Departamento de Física, Faculdade de Ciências, Universidade de Lisboa, Avenida Professor Gama Pinto 2, Lisboa 1649-003, Portugal*

[3]*Instituto de Física Téorica, Universidade Estadual Paulista, 01140-070, São Paulo, São Paulo, Brazil*

[4]*Department of Physics, Kulliyyah of Science, International Islamic University of Malaysia, Jalan Istana, Bandar Indera Mahkota 25200, Kuantan, Malaysia*

(Received 30 August 2013; published 15 November 2013)

We introduce the notion of a $\mathcal{PT}$-symmetric dimer with a $\chi^{(2)}$ nonlinearity. Similarly to the Kerr case, we argue that such a nonlinearity should be accessible in a pair of optical waveguides with quadratic nonlinearity and gain and loss, respectively. An interesting feature of the problem is that because of the two harmonics, there exist in general two distinct gain and loss parameters, different values of which are considered herein. We find a number of traits that appear to be absent in the more standard cubic case. For instance, bifurcations of nonlinear modes from the linear solutions occur in two different ways depending on whether the first- or the second-harmonic amplitude is vanishing in the underlying linear eigenvector. Moreover, a host of interesting bifurcation phenomena appear to occur, including saddle-center and pitchfork bifurcations which our parametric variations elucidate. The existence and stability analysis of the stationary solutions is corroborated by numerical time-evolution simulations exploring the evolution of the different configurations, when unstable.

DOI: 10.1103/PhysRevA.88.053820 PACS number(s): 42.65.Tg, 42.65.Ky, 42.65.Wi

I. INTRODUCTION

In the past 15 years, the remarkable original proposal of Ref. [1], relaying a potential physical relevance to Hamiltonians respecting parity- ($\mathcal{P}$) and time-reversal ($\mathcal{T}$) symmetries, has received considerable attention [2]. This proposal has highlighted the interest in considering (as operators potentially bearing real spectra) Hamiltonians that are invariant under these fundamental symmetries as an extension of the more usually considered self-adjoint Hamiltonian operators of quantum mechanics. While for a decade since their inception, these notions have been studied intensely at the linear level, especially in the mathematical community (see, e.g., the review of [2]), more recently it was realized that linear optics [3] could present an ideal playground for the realization of such non-Hermitian settings (i.e., in "open" systems bearing gain and loss but in a $\mathcal{PT}$-symmetric form). In particular, discrete systems [4,5] with balanced gain and loss have been suggested as reduced models of the non-Hermitian optics, obeying remarkable properties of waveguiding and giving origin to the blossoming field of discrete $\mathcal{PT}$-symmetric optics. $\mathcal{PT}$ symmetry was thus first studied experimentally in the optical experiments of [6–9]. As a natural extension of optical applications, the authors of Ref. [10] suggested consideration of nonlinear optical systems whose linear limit is $\mathcal{PT}$ symmetric, and in particular it was shown that such systems with a periodic potential support stable solitons.

The simplest basic element of the discrete $\mathcal{PT}$-symmetric optics is a dimer with one site subjected to dissipation and another site subjected to gain [4,5]. As a natural application of this system, one can consider a coupler with one active and one lossy waveguide [7]. When the nonlinear effects are included, one deals with a $\mathcal{PT}$-symmetric nonlinear coupler, i.e., mathematically with a $\mathcal{PT}$-symmetric nonlinear dimer. Such a dimer with a Kerr-type nonlinearity has been intensively studied, showing remarkable properties. In particular, it was shown in [11] that such a nonlinear coupler is an integrable system allowing for a solution in the form of quadratures. The effect of nonlinear suppression of periodic time reversals and beam switching to the waveguide with gain was reported in [12] (a similar switching effect can also be implemented with $\mathcal{PT}$-symmetric impurities inserted in an otherwise conservative coupler [13]).

Further studies of nonlinear discrete optical systems were performed in a number of directions. We mention a few of these in what follows. First, including one more coordinate (in addition to the evolution one; in optical applications such systems could be seen as coupled planar waveguides with balanced gain and loss) made it relevant to consider the dynamics of bright [14] and dark [15] solitons, breathers [16], as well as instabilities and rogue waves [17]. Another extension of nonlinear dimer activity is related to the inclusion of $\mathcal{PT}$-symmetric defects in discrete nonlinear systems. In the latter context, problems such as nonlinear wave scattering [18] (see also [19]) and the lifting of the degeneracy of discrete vortices [20] were considered. Finally, a nonlinear dimer or more generally the so-called nonlinear "oligomers" (i.e., few site configurations) introduced in [21] (see also [22]), were shown to allow for the existence of continuous families of nonlinear modes [23]. Among these, a $\mathcal{PT}$-symmetric quadrimer model naturally appears in the description of light propagation in a birefringent coupler [24]. Discrete solitons in different types of infinite $\mathcal{PT}$-symmetric waveguide arrays were studied numerically [25] and analytical proofs for their existence have been proposed using the anticontnuum limit [26] and via analysis of the modes bifurcating from the linear limit [27]. Solitons in a necklace of coupled dispersive waveguides were reported in [28].

Most of the above investigations have taken place at the level of the well-known Kerr-type nonlinearity. The existence of nonlinear modes and integrals of motion in $\mathcal{PT}$-symmetric

systems with more general cubic nonlinearities was investigated in [29]. Nevertheless, another type of nonlinearity of particular interest to optics is the quadratic one [30]. In the latter context, switching in two parallel waveguides was studied in [31]. Intensity-dependent switching in lithium niobate directional couplers was subsequently first observed in [32]. The particular case of a dimer with one nonlinear and one linear waveguide was considered in [33]. Furthermore, nonlinear localized modes in arrays with a quadratic nonlinearity are considered in numerous works [34–37]. Experimentally [38], the fundamental modes of a second harmonic are strongly confined, so the coupling constant between second-harmonic modes in different waveguides is very small and sometimes can even be neglected. Discrete solitary waves in this configuration were systematically probed in [39]. The plane waves and localized modes in this case were considered in [40]. Extensions in the case of two-dimensional states including discrete vortices were proposed in [41], while the mobility of the solitary waves in both one and two dimensions was explored in [42].

Recently the studies of solitons in quadratically nonlinear media were extended to $\mathcal{PT}$-symmetric systems. More specifically, the existence and stability of solitons for localized potentials in quadratic media was explored in [43]. In the work of [44], the effect of periodic $\mathcal{PT}$-symmetric potentials on $\chi^{(2)}$ solitons was described.

It is in that direction of exploring the interplay of quadratic nonlinearity and $\mathcal{PT}$-symmetric potentials that the present work is focused. It is appreciated that even in the case of two waveguides, this combination offers a significant level of complexity, as well as a number of features that are absent in the cubic Kerr nonlinearity case. In particular, due to quadratic nonlinearity and the particular structure of the eigenvectors of the underlying linear $\mathcal{PT}$-symmetric operator, continuation of the linear eigenvectors into the nonlinear domain is performed in two different ways, depending on whether the first or the second harmonic is vanishing in the linear eigenvector. We develop perturbative formal expansions that enable us to capture analytically these two different types of bifurcations of the nonlinear modes from the linear solutions. Next, we employ numerical computations and observe the symmetry breaking, as well as saddle-node bifurcations, and identify the stability characteristics of the solutions. In the case of instability, the dynamical evolution of the configurations is explored.

Our presentation is structured as follows. In Sec. II, upon introducing the general model, we focus on its linear analysis. In Sec. III, we introduce nonlinearity and analytically explore how it affects the linear modes (i.e., consider the bifurcations of nonlinear from linear modes). In Sec. IV, we corroborate our analytical considerations with detailed numerical results identifying the nonlinear modes and their stability for different values of the propagation constant and the gain and loss strength parameters. For the unstable modes, we touch upon their dynamical evolution in Sec. V. Finally, in Sec. VI, we summarize our findings and present some interesting directions for future studies.

II. THE MODEL AND ITS LINEAR ANALYSIS

The prototypical setup of equations describing the $\mathcal{PT}$-symmetric coupler with quadratic nonlinearity reads as follows:

$$i\dot{u}_1 = k_1 u_2 - 2u_1^* v_1 + i\gamma_1 u_1, \tag{1a}$$

$$i\dot{v}_1 = k_2 v_2 - u_1^2 - q v_1 + i\gamma_2 v_1, \tag{1b}$$

$$i\dot{u}_2 = k_1 u_1 - 2u_2^* v_2 - i\gamma_1 u_2, \tag{1c}$$

$$i\dot{v}_2 = k_2 v_1 - u_2^2 - q v_2 - i\gamma_2 v_2. \tag{1d}$$

Each waveguide contains two harmonics: the fundamental field (first harmonic) u_j and the second harmonic v_j, $j = 1,2$, which are nonlinearly coupled. The linear coupling between the first harmonics is characterized by the parameter k_1, and that of the second harmonics by k_2. Both k_1 and k_2 will be considered positive. The gain (loss) strength in the two arms of the dimer is given by the parameters $\gamma_j > 0$ ($\gamma_j < 0$), for the first ($j = 1$) and second ($j = 2$) harmonics, respectively. In what follows, we will explore different values of (γ_1, γ_2) to get a systematic sense of the model phenomenology. The overdot in (1) denotes the derivative with respect to the evolution variable which, here, we will denote as t (although in the optical realm it represents the propagation distance z).

Being interested in the stationary modes, we make use of the ansatz

$$\begin{pmatrix} u_1 \\ v_1 \\ u_2 \\ v_2 \end{pmatrix} = e^{-i\Lambda E t}\mathbf{w} \quad \text{where} \quad \Lambda = \begin{pmatrix} 1 & 0 & 0 & 0 \\ 0 & 2 & 0 & 0 \\ 0 & 0 & 1 & 0 \\ 0 & 0 & 0 & 2 \end{pmatrix}, \tag{2}$$

E is the propagation constant, and $\mathbf{w}$ is a 4×1 constant column vector. This reduces (1) to the eigenvalue problem

$$E\Lambda\mathbf{w} = H\mathbf{w} + F(\mathbf{w})\mathbf{w}, \tag{3}$$

with the respective linear operator given by

$$H = \begin{pmatrix} i\gamma_1 & 0 & k_1 & 0 \\ 0 & i\gamma_2 - q & 0 & k_2 \\ k_1 & 0 & -i\gamma_1 & 0 \\ 0 & k2 & 0 & -i\gamma_2 - q \end{pmatrix} \tag{4}$$

and the nonlinear part described by the matrix function

$$F(\mathbf{w}) = -\begin{pmatrix} 0 & 2(w^{(1)})^* & 0 & 0 \\ w^{(1)} & 0 & 0 & 0 \\ 0 & 0 & 0 & 2(w^{(3)})^* \\ 0 & 0 & w^{(3)} & 0 \end{pmatrix}, \tag{5}$$

where $w^{(j)}$ are used for the entries of the vector $\mathbf{w}$.

It is easy to check that H is $\mathcal{PT}$ symmetric with respect to the action of the parity operator

$$\mathcal{P} = \begin{pmatrix} 0 & 0 & 1 & 0 \\ 0 & 0 & 0 & 1 \\ 1 & 0 & 0 & 0 \\ 0 & 1 & 0 & 0 \end{pmatrix}, \tag{6}$$

and the time-reversal operator $\mathcal{T}$ performing the complex conjugation (along with $t \to -t$): $H\mathcal{PT} = \mathcal{PT}H$.

In the linear case [when one neglects all the nonlinear terms, i.e., $F(\mathbf{w})\mathbf{w}$] the problem decouples into two $\mathcal{PT}$-symmetric dimers: the first one is composed of fields u_1 and u_2 and the other of the fields v_1 and v_2. Now the eigenvalue problem (3) is reduced to $H\tilde{\mathbf{w}} = \Lambda\tilde{E}\tilde{\mathbf{w}}$, where we use the tilde in order to refer to eigenvectors and eigenvalues of the linear problem. Solutions of the latter equation can be found from the spectrum

of the operator $\Lambda^{-1}H$. The computation yields the following linear eigenvalues:

$$\tilde{E}_{1,2} = \pm\sqrt{k_1^2 - \gamma_1^2}, \quad \tilde{E}_{3,4} = \tfrac{1}{2}\big(-q \pm \sqrt{k_2^2 - \gamma_2^2}\big). \quad (7)$$

The eigenvectors associated with the eigenvalues $\tilde{E}_{1,2}$ can be written down as follows:

$$\tilde{\mathbf{w}}_1 = \begin{pmatrix} e^{i\theta_1/2} \\ 0 \\ e^{-i\theta_1/2} \\ 0 \end{pmatrix}, \quad \tilde{\mathbf{w}}_2 = \begin{pmatrix} ie^{-i\theta_1/2} \\ 0 \\ -ie^{i\theta_1/2} \\ 0 \end{pmatrix}, \quad (8)$$

while for $\tilde{E}_{3,4}$ one has

$$\tilde{\mathbf{w}}_3 = \begin{pmatrix} 0 \\ e^{i\theta_2/2} \\ 0 \\ e^{-i\theta_2/2} \end{pmatrix}, \quad \tilde{\mathbf{w}}_4 = \begin{pmatrix} 0 \\ ie^{-i\theta_2/2} \\ 0 \\ -ie^{i\theta_2/2} \end{pmatrix}, \quad (9)$$

where $\theta_{1,2} = \arctan(\frac{\gamma_{1,2}}{\sqrt{k_{1,2}^2 - \gamma_{1,2}^2}})$. Introducing the inner product as $\langle \mathbf{w}_1, \mathbf{w}_2 \rangle = \mathbf{w}_1^\dagger \mathbf{w}_2$ [hereafter $\mathbf{w}^\dagger = (\mathbf{w}^T)^*$ is the Hermitian conjugation], we observe that the linear eigenvectors obey the following relation:

$$\langle \tilde{\mathbf{w}}_j^*, \Lambda \tilde{\mathbf{w}}_p \rangle = \tilde{\mathbf{w}}_j^T \Lambda \tilde{\mathbf{w}}_p = 0, \quad j \neq p. \quad (10)$$

Notice however that $\langle \tilde{\mathbf{w}}_j^*, \Lambda \tilde{\mathbf{w}}_j \rangle \neq 0$.

Generally speaking, the existence of two different gain and loss coefficients in $\mathcal{PT}$-symmetric lattices results in the existence of different "phases" [23,29] featuring different linear properties of the model. In the case at hand the linear part of the system can belong to one of the four phases: (i) unbroken (or *exact*) $\mathcal{PT}$ symmetry when all the four eigenvalues (7) are real; this phase corresponds to the rectangle given by the inequalities $|\gamma_1| < k_1$ and $|\gamma_2| < k_2$; (ii) $\tilde{E}_{1,2}$ are complex conjugates while $\tilde{E}_{3,4}$ remain real, which corresponds to $|\gamma_1| > k_1$ and $|\gamma_2| < k_2$; (iii) vice versa, $\tilde{E}_{1,2}$ are real while $\tilde{E}_{3,4}$ are complex conjugates; this corresponds to $|\gamma_1| < k_1$ and $|\gamma_2| > k_2$; (iv) all four eigenvalues have nonzero imaginary part, i.e., $|\gamma_1| > k_1$ and $|\gamma_2| > k_2$. Phases (ii)–(iv) correspond to the broken $\mathcal{PT}$ symmetry. On the plane (γ_1, γ_2) there exist four *quadruple points* corresponding to the corners of the above-mentioned rectangle: $(\gamma_1, \gamma_2) = (\pm k_1, \pm k_2)$. These are the exceptional points where all four phases touch.

If the $\mathcal{PT}$ symmetry is unbroken, i.e., $|\gamma_1| < k_1$ and $|\gamma_2| < k_2$, then the choice of the eigenvectors in Eqs. (8) and (9) makes them $\mathcal{PT}$ *invariant*, i.e., $\mathcal{PT}\tilde{\mathbf{w}} = \tilde{\mathbf{w}}$. One can see that in the absence of the degeneracy, i.e., for all $\tilde{E}_j$ different, in the stationary linear regime the total energy is concentrated in only one harmonic of each waveguide. Namely, the field is guided only in the first (second) harmonic, i.e., $v_{1,2} = 0$ ($u_{1,2} = 0$), for the eigenvectors corresponding to the eigenvalues $\tilde{E}_{1,2}$ ($\tilde{E}_{3,4}$). This will prove rather critical in some of the considerations that follow (especially as regards the continuation of nonlinear modes from the linear limit). Notice that the linear modes $\tilde{\mathbf{w}}_3$ and $\tilde{\mathbf{w}}_4$ at the same time solve the full (i.e., the nonlinear) system (1) because in the absence of the energy guided in the fundamental mode, the system is effectively linear: $F(\tilde{\mathbf{w}}_{3,4}) = 0$.

III. BIFURCATIONS OF NONLINEAR MODES FROM THE LINEAR EIGENSTATES

In the previous section we computed solutions of the linear problem which can be formally obtained from the full nonlinear problem (3) by neglecting the nonlinear term $F(\mathbf{w})\mathbf{w}$. In this section we look for solutions of the full nonlinear problem bifurcating from the linear solutions. To this end we construct formal small-parameter expansions around the linear eigenvectors (8) and (9). However, properties of the eigenvectors $\tilde{\mathbf{w}}_{1,2}$ and $\tilde{\mathbf{w}}_{3,4}$ are essentially different: the latter couple of linear eigenvectors simultaneously solve the full nonlinear problem because the nonlinear operator vanishes at them, i.e., $F(\mathbf{w}_{3,4}) = 0$. However, for the eigenvectors $\tilde{\mathbf{w}}_{1,2}$ one has $F(\mathbf{w}_{1,2}) \neq 0$. This suggests that the formal expansions for the nonlinear modes bifurcating from $\tilde{\mathbf{w}}_{1,2}$ and $\tilde{\mathbf{w}}_{3,4}$ should be constructed in different ways.

A. Nonlinear modes bifurcating from $\tilde{\mathbf{w}}_{1,2}$

Since $F(\mathbf{w}_{1,2}) \neq 0$, one can expect that the linear solutions $\tilde{\mathbf{w}}_{1,2}$ can approximate nonlinear modes only in a situation when the nonlinear term $F(\mathbf{w})\mathbf{w}$ is negligible in Eq. (3). This situation occurs if one considers nonlinear modes $\mathbf{w}$ of small amplitude, i.e., at $\|\mathbf{w}\| \to 0$ which is usually referred to as the *linear limit* (here $\|\tilde{\mathbf{w}}\|$ stands for a norm of the vector $\tilde{\mathbf{w}}$, which could be, say, the Euclidean one). Therefore, let us search for small-amplitude nonlinear modes bifurcating from the linear solutions $\tilde{\mathbf{w}}_{1,2}$. We assume that $\mathcal{PT}$ symmetry is unbroken and all the eigenvalues (7) are distinct from each other and introduce the following formal expansions for the nonlinear modes $\mathbf{w}_j$ bifurcating from the jth linear eigenstate ($j = 1,2$):

$$\mathbf{w}_j = \varepsilon\tilde{\mathbf{w}}_j + \varepsilon^2\mathbf{W}_j^{(1)} + \varepsilon^3\mathbf{W}_j^{(2)} + \cdots, \quad (11)$$

$$E_j = \tilde{E}_j + \varepsilon e_j^{(1)} + \varepsilon^2 e_j^{(2)} + \cdots. \quad (12)$$

Here ε is a small positive formal parameter, and $\mathbf{W}_j^{(1,2,\ldots)}$ and $e_j^{(1,2,\ldots)}$ are the vectors and the coefficients to be determined. The expansion (11) and the definition (5) imply that $F(\mathbf{w}_j) = \varepsilon F(\tilde{\mathbf{w}}_j) + \varepsilon^2 F(\mathbf{W}_j^{(1)}) + \cdots$.

Since the linear eigenvectors $\tilde{\mathbf{w}}_p$ ($p = 1,2,3,4$) constitute a complete basis, we can search for the correction $\mathbf{W}_j^{(1)}$ in the form

$$\mathbf{W}_j^{(1)} = \sum_{p=1,\, p\neq j}^{4} c_p \tilde{\mathbf{w}}_p \quad (13)$$

(notice that in the latter equation we set $c_j = 0$, which can always be achieved by means of renormalization of the small parameter ε). Substituting the introduced expansions into the nonlinear problem (3), in the ε^2 order we have

$$\tilde{E}_j \Lambda \mathbf{W}_j^{(1)} + e_j^{(1)} \Lambda \tilde{\mathbf{w}}_j = H\mathbf{W}_j^{(1)} + F(\tilde{\mathbf{w}}_j)\tilde{\mathbf{w}}_j. \quad (14)$$

An unusual property of the case at hand is that the nonlinearity is orthogonal to the states $\tilde{\mathbf{w}}_j^*$ and $\tilde{\mathbf{w}}_{3-j}^*$:

$$\langle \tilde{\mathbf{w}}_j^*, F(\tilde{\mathbf{w}}_j)\tilde{\mathbf{w}}_j \rangle = \langle \tilde{\mathbf{w}}_{3-j}^*, F(\tilde{\mathbf{w}}_j)\tilde{\mathbf{w}}_j \rangle = 0. \quad (15)$$

Thus applying $\tilde{\mathbf{w}}_j^\dagger$ and $\tilde{\mathbf{w}}_{3-j}^\dagger$ to both sides of (14), using that $H^\dagger = H^*$ and $\Lambda^\dagger = \Lambda$ and accounting for (10), one readily

finds that $e_j^{(1)} = 0$ and $c_{3-j} = 0$. Finally, applying $\tilde{\mathbf{w}}_3^\dagger$ and $\tilde{\mathbf{w}}_4^\dagger$, we compute the coefficients $c_{3,4}$ explicitly, which yields the following expression:

$$\mathbf{W}_j^{(1)} = \frac{\langle \tilde{\mathbf{w}}_3^*, F(\tilde{\mathbf{w}}_j)\tilde{\mathbf{w}}_j\rangle \tilde{\mathbf{w}}_3}{(\tilde{E}_j - \tilde{E}_3)\langle \tilde{\mathbf{w}}_3^*, \Lambda\tilde{\mathbf{w}}_3\rangle} + \frac{\langle \tilde{\mathbf{w}}_4^*, F(\tilde{\mathbf{w}}_j)\tilde{\mathbf{w}}_j\rangle \tilde{\mathbf{w}}_4}{(\tilde{E}_j - \tilde{E}_4)\langle \tilde{\mathbf{w}}_4^*, \Lambda\tilde{\mathbf{w}}_4\rangle}. \quad (16)$$

Proceeding to the next order of the expansions, at ε^3 we obtain

$$\tilde{E}_j \Lambda \mathbf{W}_j^{(2)} + e_j^{(2)} \Lambda \tilde{\mathbf{w}}_j = H\mathbf{W}_j^{(2)} + F(\tilde{\mathbf{w}}_j)\mathbf{W}_j^{(1)}, \quad (17)$$

where we have used (16) and the property $F(\tilde{\mathbf{w}}_3) = F(\tilde{\mathbf{w}}_4) = 0$ yielding $F(\mathbf{W}_j^{(1)}) = 0$. Thus applying $\tilde{\mathbf{w}}_j^\dagger$ to (17), we compute (recall $j = 1,2$)

$$e_j^{(2)} = \frac{1}{\langle \tilde{\mathbf{w}}_j^*, \Lambda\tilde{\mathbf{w}}_j\rangle} \sum_{p=3,4} \frac{\langle \tilde{\mathbf{w}}_p^*, F(\tilde{\mathbf{w}}_j)\tilde{\mathbf{w}}_j\rangle \langle \tilde{\mathbf{w}}_j^*, F(\tilde{\mathbf{w}}_j)\tilde{\mathbf{w}}_p\rangle}{(\tilde{E}_j - \tilde{E}_p)\langle \tilde{\mathbf{w}}_p^*, \Lambda\tilde{\mathbf{w}}_p\rangle}. \quad (18)$$

Formulas (16) and (18) determine the required terms of the expansions.

B. Nonlinear modes bifurcating from $\tilde{\mathbf{w}}_{3,4}$

As mentioned above in our specific case $F(\tilde{\mathbf{w}}_{3,4}) = 0$ and thus the linear eigenvectors $\tilde{\mathbf{w}}_{3,4}$ at the same time solve the original nonlinear model (3). This means that the nonlinear modes (if any) bifurcating from $\tilde{\mathbf{w}}_{3,4}$ should in general possess finite nonzero amplitude at the point of the bifurcation. In other words, the bifurcations of nonlinear modes $\mathbf{w}$ occur not from the linear limit (which is understood as $\|\mathbf{w}\| \to 0$), but rather from a finite amplitude solution (see also the discussion in [43, 44]). This readily suggests that the small-parameter expansions for nonlinear modes bifurcating from $\tilde{\mathbf{w}}_{3,4}$ should be looked for as follows ($j = 3,4$):

$$\mathbf{w}_j = \alpha_j \tilde{\mathbf{w}}_j + \varepsilon \mathbf{W}_j^{(1)} + \varepsilon^2 \mathbf{W}_j^{(2)} + \cdots, \quad (19)$$

$$E_j = \tilde{E}_j + \varepsilon e_j^{(1)} + \varepsilon^2 e_j^{(2)} + \cdots, \quad (20)$$

where we have introduced the proportionality coefficients α_j, which must be defined from the requirement of consistency of the asymptotic expansion. Notice that if $\alpha_j \neq 0$, then at the point of bifurcation (i.e., at $\varepsilon = 0$), the power of the first harmonic goes to zero, i.e., $|w_j^{(1,3)}| = 0$, while $|w_j^{(2,4)}|$ stay finite.

Now one has $F(\mathbf{w}_j) = \varepsilon F(\mathbf{W}_j^{(1)}) + \varepsilon^2 F(\mathbf{W}_j^{(2)}) + \cdots$. Substituting the introduced expansions into the nonlinear problem (3), we observe that it is automatically satisfied in the leading order ε^0. In the ε^1 order for $j = 3,4$ we obtain

$$\alpha_j e_j^{(1)} \Lambda \tilde{\mathbf{w}}_j + \tilde{E}_j \Lambda \mathbf{W}_j^{(1)} = H\mathbf{W}_j^{(1)} + \alpha_j F\big(\mathbf{W}_j^{(1)}\big)\tilde{\mathbf{w}}_j. \quad (21)$$

Employing again the representation (13) [recall that $F(\mathbf{w}_{3,4}) = 0$] we find $F(\mathbf{W}_j^{(1)}) = c_1 F(\tilde{\mathbf{w}}_1) + c_2 F(\tilde{\mathbf{w}}_2)$. Applying $\tilde{\mathbf{w}}_{7-j}^\dagger$ to both sides of (21) and using properties (10) and

$$\langle \tilde{\mathbf{w}}_j^*, F(\tilde{\mathbf{w}}_{1,2})\tilde{\mathbf{w}}_j\rangle = \langle \tilde{\mathbf{w}}_{7-j}^*, F(\tilde{\mathbf{w}}_{1,2})\tilde{\mathbf{w}}_j\rangle = 0, \quad (22)$$

we find that $c_{7-j} = 0$. Next, we apply $\tilde{\mathbf{w}}_j^\dagger$ and using the same arguments find that $e_j^{(1)} = 0$. Finally, we apply $\tilde{\mathbf{w}}_1^\dagger$ and $\tilde{\mathbf{w}}_2^\dagger$ which yields the following system:

$$c_1\langle \tilde{\mathbf{w}}_1^*, \Lambda\tilde{\mathbf{w}}_1\rangle(\tilde{E}_j - \tilde{E}_1) - \alpha_j c_1 \langle \tilde{\mathbf{w}}_1^*, F(\tilde{\mathbf{w}}_1)\tilde{\mathbf{w}}_j\rangle - \alpha c_2 \langle \tilde{\mathbf{w}}_1^*, F(\tilde{\mathbf{w}}_2)\tilde{\mathbf{w}}_j\rangle = 0, \quad (23)$$

$$c_2\langle \tilde{\mathbf{w}}_2^*, \Lambda\tilde{\mathbf{w}}_2\rangle(\tilde{E}_j - \tilde{E}_2) - \alpha_j c_1 \langle \tilde{\mathbf{w}}_2^*, F(\tilde{\mathbf{w}}_1)\tilde{\mathbf{w}}_j\rangle - \alpha_j c_2 \langle \tilde{\mathbf{w}}_2^*, F(\tilde{\mathbf{w}}_2)\tilde{\mathbf{w}}_j\rangle = 0. \quad (24)$$

For a given $j = 3,4$ the latter equations form a homogeneous linear system with respect to the coefficients c_1 and c_2. The compatibility condition of this system results in a *quadratic* equation with respect to α_j whose roots give admissible values of α_j in (19). If α_j is chosen to satisfy the compatibility condition, then the coefficients of c_1 and c_2 are given up to a multiplier, which however can be scaled out by means of renormalization of the small parameter ε.

In order to determine $e_j^{(2)}$ one can proceed to the ε^2 order, which yields

$$\alpha_j e_j^{(2)} \Lambda \tilde{\mathbf{w}}_j + \tilde{E}_j \Lambda \mathbf{W}_j^{(2)} = H\mathbf{W}_j^{(2)} + \alpha_j F\big(\mathbf{W}_j^{(2)}\big)\tilde{\mathbf{w}}_j + \alpha_j F\big(\mathbf{W}_j^{(1)}\big)\mathbf{W}_j^{(1)}. \quad (25)$$

After applying $\tilde{\mathbf{w}}_j^\dagger$ one finds

$$e_j^{(2)} = \frac{1}{\alpha_j \langle \tilde{\mathbf{w}}_j^*, \Lambda\tilde{\mathbf{w}}_j\rangle} \sum_{p=1}^{2}\sum_{q=1}^{2} c_p c_q \langle \tilde{\mathbf{w}}_j^*, F(\tilde{\mathbf{w}}_p)\tilde{\mathbf{w}}_q\rangle, \quad (26)$$

which gives the leading-order correction to the propagation constant.

C. Discussion

The results of Secs. III A and III B show that due to the interplay between the quadratic nonlinearity and the particular structure of the eigenvectors of the underlying linear problem, continuation of the linear eigenvectors into the nonlinear domain occurs in two different ways, depending on whether the second or the first harmonic is vanishing in the linear eigenvector. In the first case, when the total energy of the linear eigenvectors $\tilde{\mathbf{w}}_{1,2}$ is fully concentrated in the first harmonic, the bifurcations of nonlinear solutions from the linear ones resemble the standard Kerr nonlinearity case: each linear eigenstate produces one family of nonlinear modes, and at the point of the bifurcation ($\varepsilon = 0$) the amplitude of the nonlinear modes is zero, gradually increasing when one passes from $\varepsilon = 0$ to small nonzero ε. Therefore, the bifurcations occur from the linear limit.

However, in the second situation, when the linear eigenvectors $\tilde{\mathbf{w}}_{3,4}$ have a vanishing first-harmonic contribution and a nonvanishing second-harmonic one, the bifurcations of nonlinear modes occur in another way. Now, at the point of bifurcation ($\varepsilon = 0$), the nonlinear modes generically bear a finite nonzero amplitude due to the presence of the additional term with the coefficient α_j. Moreover, since the possible values of α_j are given by the quadratic equation, each linear eigenstate in general creates at least two physically distinct families of nonlinear modes. Finally we notice that we have computed values of α_j for several choices of model parameters, obtaining in this way an analytical prediction for the amplitude of nonlinear modes at the point of bifurcation ($\varepsilon = 0$). For

all cases that we checked we observed that the analytically predicted amplitude of the bifurcating nonlinear modes agrees with that obtained from the direct numerical results that follow in Sec. IV.

IV. FULLY NONLINEAR MODES

A. Theoretical setup

Going beyond the consideration of the nonlinear modes described by the expansions (11), (12) and (19), (20), let us now turn to the set of all stationary nonlinear modes obeying the system (3). We observe that the latter system has a considerable wealth of solutions of which we provide a representative set in what follows. In particular, we focus on nonlinear solutions preserving the symmetry pertinent to the linear part, i.e., to the $\mathcal{PT}$-invariant modes obeying $\mathcal{PT}\mathbf{w} = \mathbf{w}$. Using for such modes the amplitude-phase decomposition we rewrite the stationary solution $\mathbf{w}$ introduced by (2) in the form

$$\mathbf{w} = \begin{pmatrix} Ae^{i\phi_1} \\ Be^{i\phi_2} \\ Ae^{-i\phi_1} \\ Be^{-i\phi_2} \end{pmatrix}, \tag{27}$$

where A and B are real stationary amplitudes and $\phi_{1,2}$ are stationary phases. This ansatz reduces (3) to a system of stationary equations as follows:

$$E = k_1 e^{-2i\phi_1} - 2Be^{i(\phi_2-2\phi_1)} + i\gamma_1, \tag{28a}$$

$$2E = k_2 e^{2i\phi_2} - (A^2/B)e^{i(\phi_2-2\phi_1)} - q - i\gamma_2 \tag{28b}$$

(where it is assumed that $B \neq 0$). Further splitting to real and imaginary parts yields four equations:

$$E = k_1 \cos(2\phi_1) - 2B\cos(\phi_2 - 2\phi_1), \tag{29a}$$

$$0 = -k_1 \sin(2\phi_1) - 2B\sin(\phi_2 - 2\phi_1) + \gamma_1, \tag{29b}$$

$$2E = k_2 \cos(2\phi_2) - (A^2/B)\cos(\phi_2 - 2\phi_1) - q, \tag{29c}$$

$$0 = k_2 \sin(2\phi_2) - (A^2/B)\sin(\phi_2 - 2\phi_1) - \gamma_2. \tag{29d}$$

If we take A, B, and $\phi_{1,2}$ as four unknowns in the system (29), then one can expect that there exists one or several solutions for any given E. Therefore, we can speak about *continuous families* of nonlinear modes. In order to visualize these families, one can introduce the quantity

$$U = \langle \mathbf{w}, \Lambda\mathbf{w} \rangle = \mathbf{w}^\dagger \Lambda \mathbf{w} \tag{30}$$

which corresponds to the Manley-Rowe invariant (of the conservative system $\gamma_{1,2} = 0$ where it is a conserved quantity). In the case at hand we have $U = 2(A^2 + 2B^2)$. Then the families of the nonlinear modes can be displayed as dependencies on the (E,U) plane as the functions U vs E.

B. Numerical results

Several examples are presented in Fig. 1 where we first address the situation $\gamma_{1,2} = 0$ corresponding to the conservative limit of the problem and then consider the effect of nonzero $\mathcal{PT}$-symmetric components $\gamma_{1,2}$ for some representative value pairs.

The nonlinear system (29) features several interesting properties. First, as was predicted above there exist families bifurcating from the linear eigenstates $\tilde{\mathbf{w}}_{1,2}$ [see Eqs. (7) and (8)], one family bifurcating from each eigenstate. In accordance with the expansions (11), (12), at the points of the bifurcations ($\varepsilon = 0$) one has $E = \tilde{E}_{1,2}$ and $U = 0$. The modes obeying expansions (19), (20) have also been found in our numerics. For such modes at $\varepsilon = 0$ one has $E = \tilde{E}_{3,4}$ and $U = 4\alpha_{3,4}^2$ with $\alpha_{3,4}$ being solutions of the quadratic equation introduced in Sec. III B [in order to obtain the latter equality we used Eqs. (9) for the explicit form of the eigenvectors $\tilde{\mathbf{w}}_{3,4}$]. In all the considered cases we have found two distinct families bifurcating either from $\tilde{E}_3$ or from $\tilde{E}_4$. Notice, however, that the two families bifurcating from $\tilde{E}_4$ for $\gamma_{1,2} = 0$ are not distinguishable in Fig. 1(a). This is because for each given E the modes belonging to those families are mutually complex conjugate. Therefore, these solutions have the same U characteristic. They also have the identical stability properties (see below for the discussion on stability) which allows us to consider only one family of those two in what follows.

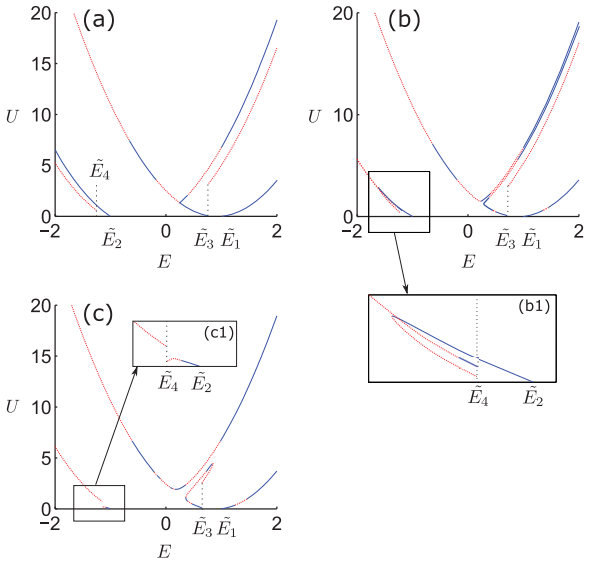

FIG. 1. (Color online) Families of nonlinear modes on the plane U vs E. The values of the parameters are given as $k_1 = 1$, $k_2 = 2$, $q = 0.5$, and $\gamma_{1,2} = 0$ (a); $\gamma_1 = 0.1$ and $\gamma_2 = 0.5$ (b); $\gamma_1 = 0.1$ and $\gamma_2 = 0.9$ (c). Stable and unstable modes correspond to the blue (solid) and red (dashed) fragments of the curves. Insets (b1) and (c1) provide better resolution for some bifurcational features not easily visible in the main plots.

It is also important to indicate that in all cases addressed in Fig. 1, the values of the parameters $\alpha_{3,4}$ allowing for the bifurcations from $\tilde{E}_{3,4}$ are distinct from zero. Therefore, the value $U = 4\alpha_{3,4}^2$ corresponding to the point of bifurcation is also distinct from zero. The latter comment is relevant because in all three panels of Fig. 1 one can observe that one of the families emerging at $E = \tilde{E}_3$ closely approaches the horizontal axis $U = 0$. However, as the above analysis clearly indicates, the relevant bifurcation point is still distinct from $U = 0$.

In terms of gross features of the bifurcation diagrams, we observe that the families are extended to the domains of either positive or negative E, and some families feature a parabolic-shaped pattern. We also notice that an apparent pitchfork bifurcation existing in Fig. 1(a) with $\gamma_{1,2} = 0$ breaks into a pair of "fold points," as we deviate from the Hamiltonian limit. Additional such fold points can be observed, e.g., in

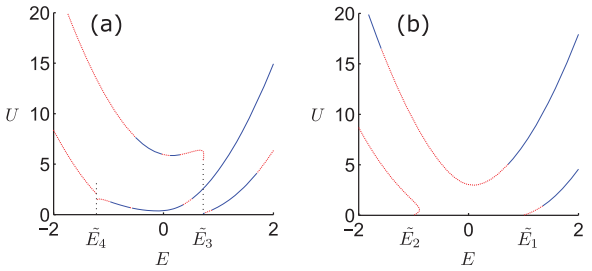

FIG. 2. (Color online) Families of nonlinear modes on the planes U vs E when the $\mathcal{PT}$ symmetry of the underlying linear problem is broken. (a) Regime (ii) with $\gamma_1 = 1.1$ and $\gamma_2 = 0.5$; (b) regime (iii) with $\gamma_1 = 0.1$, $\gamma_2 = 2.1$ [see Sec. II for definition of the regimes (ii) and (iii)]. All other parameters are the same as in Fig. 1. Notice that the eigenvalues $\tilde{E}_{1,2}$ are complex in (a), while $\tilde{E}_{3,4}$ are complex in (b).

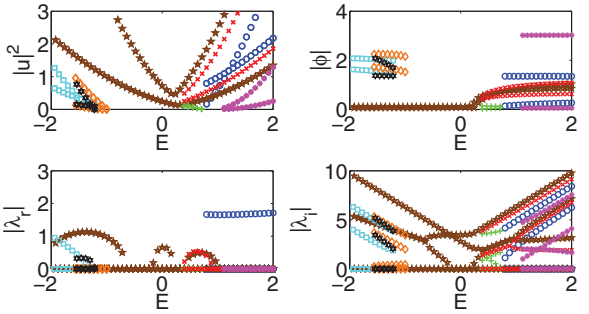

FIG. 3. (Color online) Existence and stability properties of nonlinear modes with $k_1 = 1$, $k_2 = 2$, $q = 0.5$, $\gamma_1 = 0.1$, and $\gamma_2 = 0.5$. The four panels denote the solution amplitude (top left), phase differences between adjacent nodes (top right), and the real and imaginary parts (second row) of the eigenvalues. For a detailed explanation of the different families, see the text.

Fig. 1(c) for $E \approx 0.85$, or in Fig. 1(b) for $E \approx -1.63$ [see inset (b1)]. However, it is evident that most families in the figure either come from $-\infty$ or asymptote towards $+\infty$, for large values of U.

In Fig. 1 we also address the stability of the modes obtained by means of identification of the spectrum of the linearization of the original equations. One can observe that the stability situation may be fairly complicated, with the same family having alternating domains of stability and instability (these will be analyzed in detail below for the parameters used). The linearization spectrum contains a double zero eigenvalue (due to the global phase invariance of the full model). Instability can be caused either by a pair of purely real eigenvalues in the spectrum (one of them is responsible for instability) or by a quartet of complex eigenvalues (two of which correspond to unstable modes).

Quite remarkably, nonlinear modes (including stable ones) can also be found in the regime where the $\mathcal{PT}$ symmetry of the underlying linear problem is broken. This is a feature that nonlinearity has been shown to sustain even in the cubic case, in particular for a quadrimer setting (see, e.g., the relevant discussion of [21,23]). Two examples are shown in Fig. 2. The respective parameters correspond to the underlying linear problem belonging to two different "phases" of the broken $\mathcal{PT}$ symmetry (see Sec. II). Namely, the system belongs to the phase (ii) for Fig. 2(a) while Fig. 2(b) corresponds to the phase (iii). Correspondingly, in the situation of panel (a) the eigenvalues $\tilde{E}_{1,2}$ are complex (with nonzero imaginary parts) and do not allow for bifurcations of nonlinear modes. However, the eigenvalues $\tilde{E}_{3,4}$ are still real and create the families of solutions (two families emerge at $\tilde{E}_3$ and at $\tilde{E}_4$). Vice versa, in panel (b) the eigenvalues $\tilde{E}_{3,4}$ are complex but one can observe families bifurcating from the real eigenvalues $\tilde{E}_{1,2}$ (one family from each eigenvalue). Solutions arising from $\tilde{E}_{1,2}$ are unstable in the vicinity of the bifurcations, but sufficiently strong nonlinearity in this case is critical for enabling dynamical stability. Practically, it also appears that the modes where the Manley-Rowe invariant has a positive slope have a wider stability interval, although a more quantitative observation along these lines is, presently, absent.

We now turn to a more systematic analysis of the existence and stability properties of the different families of solutions identified previously, for reasons of completeness. Figure 3 illustrates the situation where $k_1 = 1$, $k_2 = 2$, $q = 0.5$, $\gamma_1 = 0.1$, and $\gamma_2 = 0.5$. There are eight families of solutions in this case, denoted by different symbols. Their eigenvalues for the respective parameters of existence are shown in the case of three different choices of E in Fig. 4.

(a) The family denoted by blue circles arises from $E = \tilde{E}_3 \approx 0.72$ and continues monotonically increasing its Manley-Rowe diagnostic upon increase of E to infinity. It always has two pairs of purely imaginary and one pair of real eigenvalues, which give rise to its instability.

(b) The brown pentagram family exists for all the considered values of E. The amplitudes of both harmonics reach their minimum (within the parabolic shape of the family reported previously) in the interval $E \in [0.2, 0.3]$, but at different points. This family has three pairs of purely imaginary eigenvalues, two of which collide at $E \approx -2.13$ and turn into a complex quartet. At $E \approx -0.65$, the complex quartet collides on the imaginary axis and splits anew into two pairs of imaginary eigenvalues, restabilizing the waveform. The larger of the two imaginary pairs subsequently meets the largest imaginary eigenvalues and the collision yields

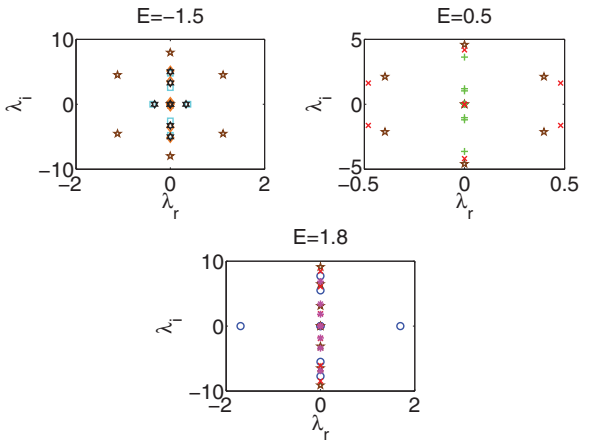

FIG. 4. (Color online) Eigenvalues of the linearization problem of nonlinear modes with $k_1 = 1$, $k_2 = 2$, $q = 0.5$, $\gamma_1 = 0.1$, and $\gamma_2 = 0.5$. The same notation has been used as in Fig. 3.

a complex quartet within the short parametric interval of $E \in [-0.20,-0.19]$ (hereafter the boundaries of the intervals are given approximately). The remaining (lowest-frequency) pair collides with the spectral plane origin and turns into a real pair at $E \approx -0.2$. This pair of eigenvalues becomes imaginary again shortly at $E \approx 0.2$ and collides with its former partner at $E \approx 0.41$ to form a complex quartet. This complex quartet once again splits into two purely imaginary pairs at $E \approx 1$. As a result, the brown pentagram family is stable for all E except on $[-2.13,-0.65],[-0.2,0.2],[0.41,1]$. From the above, the substantial complexity of the family stability properties should be rather evident.

(c) The green pluses and the red crosses arise together from a saddle-node bifurcation at $E \approx 0.3$. The green plus family is essentially stable except when E is within a small interval of $[0.47,0.48]$, where two out of three pairs of purely imaginary eigenvalues collide yielding a Hamiltonian-Hopf bifurcation and a complex quartet and the reverse path renders the eigenvalues purely imaginary again. This family terminates at $E = \tilde{E}_3 \approx 0.72$ with the first-harmonic amplitude vanishing.

(d) The family of red crosses bifurcates from the same point as the green pluses; however, it does not terminate. It is unstable only on an interval of $E \in [0.39,0.89]$ due to a complex quartet.

(e) The magenta star family arises from the linear limit at $E = \tilde{E}_1 \approx 0.99$ and exists always thereafter. It has three pairs of purely imaginary eigenvalues, too. Two of them turn into a complex quartet within the small interval $[1.38,1.43]$ and make the family unstable in this interval.

(f) The family of cyan squares comes from $-\infty$ having a real pair and two purely imaginary pairs of eigenvalues. This branch is stable only after $E \approx -1.3$ where the real pair turns purely imaginary; subsequently the branch terminates at $E = \tilde{E}_4 \approx -1.22$ (with the first-harmonic amplitude vanishing).

(g) The orange diamonds and the black hexagrams emerge from a saddle-node bifurcation at $E \approx -1.63$. The orange diamonds constitute the only family that is always stable, having three pairs of purely imaginary eigenvalues. This family terminates at the linear limit of $E = \tilde{E}_2 \approx -0.99$.

(h) The black hexagrams start at the same point as the orange diamonds but terminate at $E = \tilde{E}_4 \approx -1.22$. This family always has two pairs of purely imaginary and one pair of real eigenvalues. Hence it is generically unstable.

As general comments we can infer that, arguably, the most robust families and those that will generically exist are the ones emerging from the eigenvalues $\tilde{E}_{1,2}$ of the linear limit. The other families may have intervals of stability but also often suffer oscillatory or real instabilities and are subject to saddle-center bifurcations (although, e.g., the family starting from $\tilde{E}_1 \approx 0.99$ also has a small interval of instability, and the generically stable family starting from $\tilde{E}_2 \approx -0.99$ is subject to a saddle-node bifurcation).

Figures 5 and 6 show us the solution profiles and their eigenvalues under the parameters $k_1 = 1$, $k_2 = 2$, $q = 0.5$, $\gamma_1 = 0.1$, and $\gamma_2 = 0.9$. In this case there are seven families. The black hexagram family of Fig. 3 does not exist any more. We briefly summarize the difference in each family in the following compared with the previous ones.

(a) The red cross family now arises from a saddle-node bifurcation with the green pluses at $E \approx 0.36$ and terminates

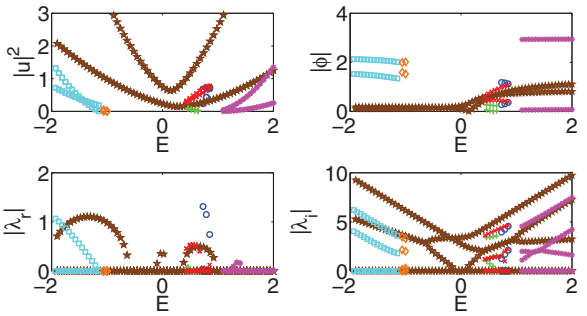

FIG. 5. (Color online) Existence and stability properties of nonlinear modes with similar settings as in Fig. 3 but for $k_1 = 1$, $k_2 = 2$, $q = 0.5$, $\gamma_1 = 0.1$, and $\gamma_2 = 0.9$.

into another saddle-node bifurcation with the blue circle families at $E \approx 0.85$. It now has a pair of purely imaginary and a complex quartet of eigenvalues. The latter reshapes into two pairs of purely imaginary eigenvalues at $E \approx 0.74$, and one of them becomes real at $E \approx 0.84$. Hence, it is unstable except on the interval $[0.74,0.84]$.

(b) The blue circle branch is still unstable but now exists from $E = \tilde{E}_3 \approx 0.64$ to $E \approx 0.85$.

(c) The green plus branch now exists from $E \approx 0.36$ to $\tilde{E}_3 \approx 0.64$. It is essentially stable except when E is in the range $[0.4,0.46]$.

(d) The brown pentagrams still exist for all E and bear similar eigenvalues as in Fig. 3. In this case, the branch is stable except on $[-2.06,-0.61],[-0.22,-0.17]$, $[-0.1,0.07],[0.37,0.97]$.

(e) The magenta star family is similar as in Fig. 3, again bifurcating from the linear limit and now being stable in the exception of the interval $E \in [1.27,1.45]$.

(f) The unstable family of cyan squares still comes from $-\infty$, but now it is always unstable and terminates at $\tilde{E}_4 = -1.14$.

(g) The orange diamond family exists from $\tilde{E}_4 \approx -1.14$ to $\tilde{E}_2 \approx -0.99$. It is unstable until $E \approx -1.1$ and becomes stable thereafter.

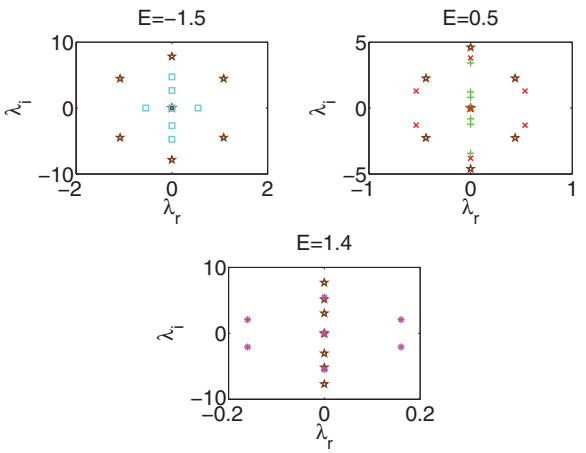

FIG. 6. (Color online) Eigenvalues of the linearization problem of nonlinear modes with $k_1 = 1$, $k_2 = 2$, $q = 0.5$, $\gamma_1 = 0.1$, and $\gamma_2 = 0.9$.

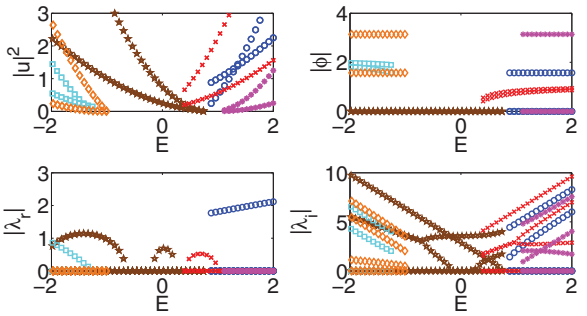

FIG. 7. (Color online) Existence and stability properties of nonlinear modes with similar settings as Fig. 3 but for $k_1 = 1, k_2 = 2$, $q = 0.5$, $\gamma_1 = 0$, and $\gamma_2 = 0$.

For comparison purposes, we also consider the Hamiltonian case $k_1 = 1$, $k_2 = 2$, $q = 0.5$, $\gamma_1 = 0$, and $\gamma_2 = 0$. Figures 7 and 8 show the six families of nonlinear modes in this case.

(a) The blue circle family is similar to the one in Fig. 3, i.e., it arises from $E = \tilde{E}_3 = 0.75$ and is always unstable. It possesses a pair of real and two pairs of purely imaginary eigenvalues for all E where it exists.

(b) The brown pentagrams now exist only up to $\tilde{E}_3 = 0.75$. This branch is stable except on $[-2.17, -0.66], [-0.17, 0.24]$, where it has a complex quartet of eigenvalues.

(c) The red crosses now bifurcate from the brown pentagrams at $E \approx 0.25$ and persist beyond the point. It is this bifurcation that apparently splits into two fold points in the two cases considered previously. The red crosses are unstable only on the interval $[0.41, 1]$, where a complex quartet of eigenvalues comes from two pairs of purely imaginary ones colliding at $E \approx 0.41$ and returning to the imaginary axis at $E \approx 1$.

(d) The magenta star family still arises from the linear limit at $\tilde{E}_1 = 1$. However, it now always has three pairs of purely imaginary eigenvalues and hence is stable wherever it exists.

(e) The cyan square family is similar to the one in Fig. 3, too. It is unstable, comes from $-\infty$, and terminates at $\tilde{E}_4 = -1.25$.

(f) The orange diamond branch now also exists from $-\infty$ and terminates at $\tilde{E}_2 = -1$. It is always stable in this case, too, again verifying the robustness of the families that emerge from the linear limit.

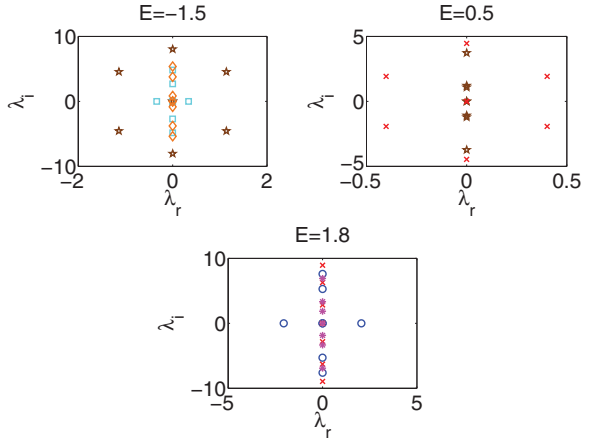

FIG. 8. (Color online) Eigenvalues of the linearization problem of nonlinear modes with $k_1 = 1, k_2 = 2, q = 0.5, \gamma_1 = 0$, and $\gamma_2 = 0$.

V. DYNAMICS OF THE SYSTEM

Finally, from the point of view of numerical results, we have also performed direct numerical simulations of the propagation dynamics of the quadratically nonlinear $\mathcal{PT}$-symmetric dimer. These simulations allow us to obtain a feeling about the dynamical implications of the instabilities presented above.

In Fig. 9, we show the dynamics of the nonlinear modes with $k_1 = 1$, $k_2 = 2$, $q = 0.5$, $\gamma_1 = 0.1$, and $\gamma_2 = 0.5$, which corresponds to Fig. 3. We choose different values of E for the different families, usually in order to simulate their typical unstable behavior under a small perturbation by numerical

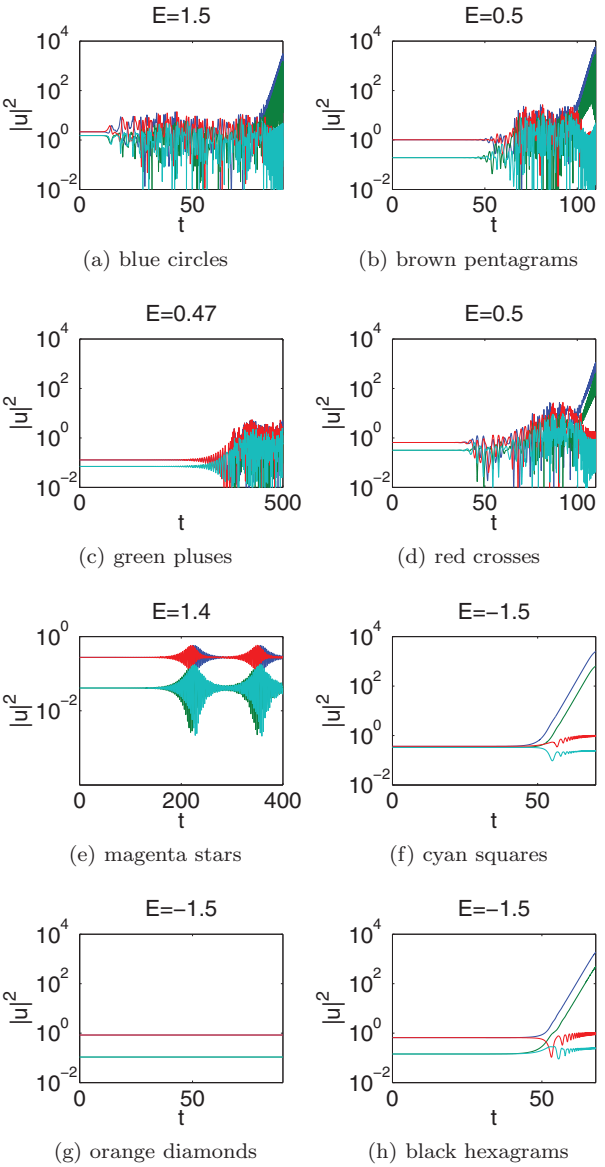

(a) blue circles (b) brown pentagrams
(c) green pluses (d) red crosses
(e) magenta stars (f) cyan squares
(g) orange diamonds (h) black hexagrams

FIG. 9. (Color online) Dynamical plots in a semilogarithmic scale for the y variable (denoting the amplitudes of the fundamental and the second harmonic) for different nonlinear modes with $k_1 = 1, k_2 = 2$, $q = 0.5, \gamma_1 = 0.1$, and $\gamma_2 = 0.5$. The family considered and the value of the propagation constant are depicted explicitly in each panel.

errors up to 10^{-7} [however, as an exception for the orange diamonds, e.g., of Fig. 9(g), we only confirm their generic stability]. In Figs. 9(a), 9(b), and 9(d), we pick $E = 1.5$ for the blue circle family, $E = 0.5$ for the brown pentagram family, and the red crosss family, where all of them are unstable. In all three cases here, the amplitudes of the first waveguide (which features gain) grow exponentially fast after some oscillation. The amplitudes of the second waveguide (which sustains loss) keep oscillating but also appear to increase in comparison to their initial values. In Fig. 9(c), all the amplitudes of the green plus family are relatively constant for a long evolution interval and oscillating around their initial values, due to its short-living complex quartet of eigenvalues at $E = 0.47$. Figure 9(e) shows the amplitudes of the two waveguides of the magenta star family which are oscillating quasiperiodically in a similar way at $E = 1.4$. Figures 9(f) and 9(h) illustrate the instability of the cyan squares and black hexagrams where the amplitudes of both harmonics of the first waveguide grow exponentially at about $t = 50$ while the amplitudes of the second waveguide do not appear to grow indefinitely (but contrary to the cubic case, they are also not observed to systematically decay [27]). The stable dynamics of the orange diamond family at $E = -1.5$ is also plotted in Fig. 9(g). Generally, for the unstable families, we infer either a growth in the first waveguide coupled with a bounded oscillation in the second waveguide, or a bounded evolution in both waveguides.

Figure 10 shows similar dynamic plots corresponding to the families plotted in Fig. 5. Here all of the blue circles, brown pentagrams, green pluses, and red crosses in panels (a)–(d) are unstable and present similar features as before, with unbounded growth in the one waveguide (but no decay of amplitude in the second). The amplitudes of the magenta stars still oscillate quasiperiodically around their initial values. In Figs. 10(f) and 10(g), both amplitudes of the first waveguide grow exponentially. The amplitudes of the second waveguide in the cyan squares decay a little and then feature a weak oscillation around their initial values, whereas for the orange diamond family they grow a little and then feature a similar weak oscillation.

Figure 11 shows the dynamics of the Hamiltonian case under the parameters $k_1 = 1$, $k_2 = 2$, $q = 0.5$, $\gamma_1 = 0$, and $\gamma_2 = 0$ that corresponds to Fig. 7. Since $\gamma_1 = 0$ and $\gamma_2 = 0$, neither of the two waveguides has a gain or loss profile. Shown

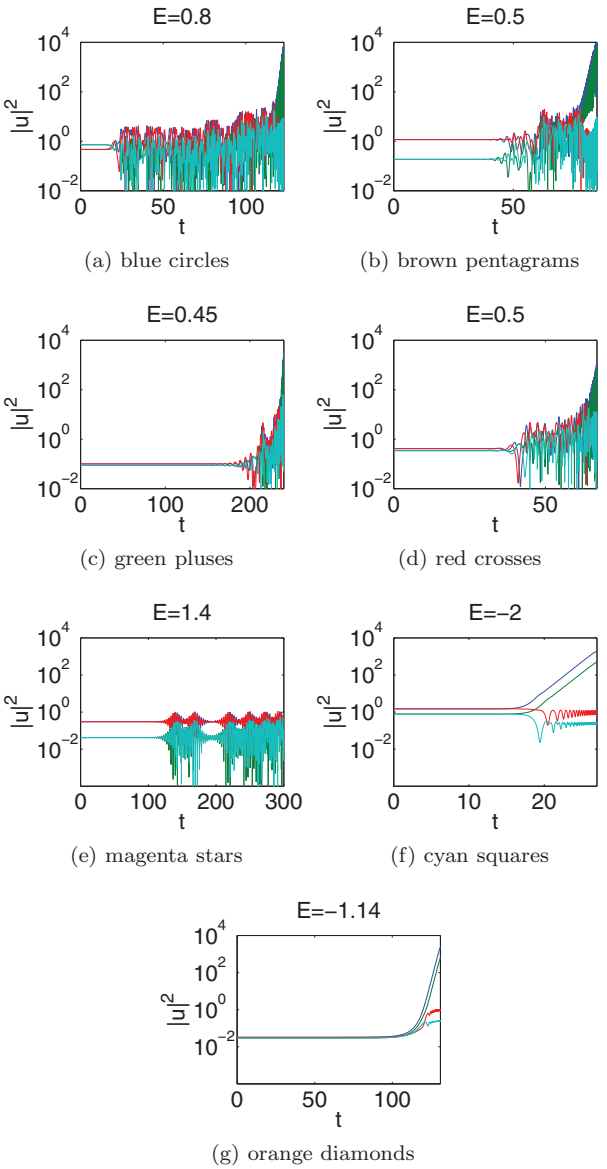

(a) blue circles (b) brown pentagrams
(c) green pluses (d) red crosses
(e) magenta stars (f) cyan squares
(g) orange diamonds

FIG. 10. (Color online) Dynamical plots in a semilogarithmic scale for the y variable (denoting the amplitudes of the fundamental and the second harmonic) for different nonlinear modes with $k_1 = 1$, $k_2 = 2$, $q = 0.5$, $\gamma_1 = 0.1$, and $\gamma_2 = 0.9$.

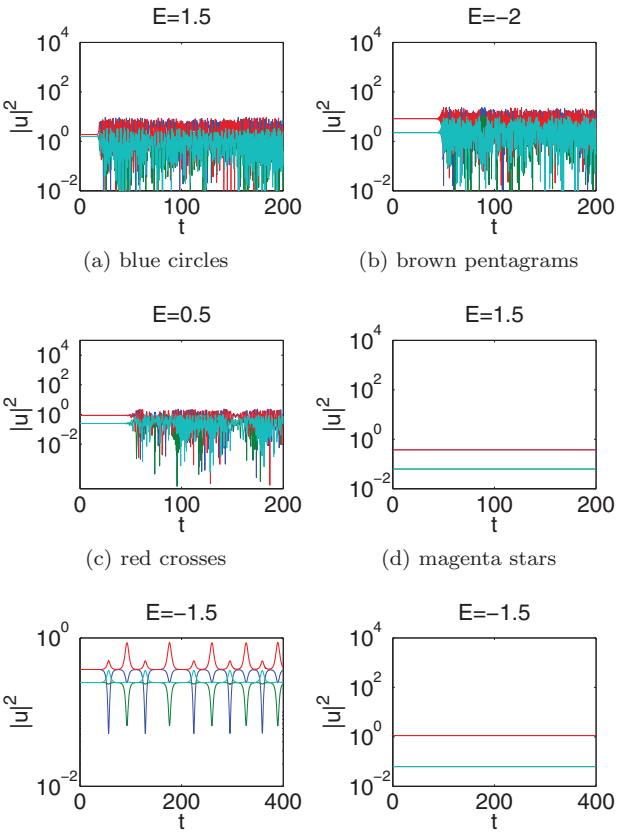

(a) blue circles (b) brown pentagrams
(c) red crosses (d) magenta stars
(e) cyan squares (f) orange diamonds

FIG. 11. (Color online) Dynamical semilogarithmic plots of nonlinear modes with $k_1 = 1$, $k_2 = 2$, $q = 0.5$, $\gamma_1 = 0$, and $\gamma_2 = 0$.

in panels (a)–(c), are all the amplitudes of the harmonics of the the blue circle, brown pentagram, and red cross families which are oscillating around their initial values, with no trend of indefinite growth or decay, just as expected by the absence of $\mathcal{PT}$-symmetric terms. In Fig. 11(e), the cyan square family amplitudes now weakly oscillate periodically (but in a way preserving as they should the Manley-Rowe invariant). Figures 11(d) and 11(f) show the stable dynamics of the magenta star and the orange diamond families in this case, i.e., confirming the dynamical robustness of the families stemming from the linear limit.

VI. CONCLUSIONS AND FUTURE WORK

In the present work, we considered systematically the features of stationary states of a prototypical $\mathcal{PT}$-symmetric quadratically nonlinear dimer (or coupler). We explored different parametric regimes in the two-dimensional plane of gain and loss (for the first and the second harmonics) and in each considered case we identified families of nonlinear modes and addressed the stability and dynamics of the solutions. We found numerous unexpected features that distinguish this system, e.g., from its more well-studied sibling, namely, the cubic $\mathcal{PT}$-symmetric nonlinear dimer.

We started our analysis by considering the spectrum of the underlying linear problem and found that its eigenvalues always have total energy fully concentrated either in the first or in the second harmonic of the waveguide. Turning to the full nonlinear problem, we have established that the found linear solutions produce nonlinear modes which (in the vicinity of the bifurcation from linear eigenstate) can be described by means of the small-parameter formal expansions. We have further revealed two types of bifurcations of nonlinear modes from the linear solutions. Namely, the nonlinear modes continued from the linear eigenvectors with total energy concentrated in the first harmonic have zero value of the Manley-Rowe characteristic at the point of bifurcation. On the other hand, the nonlinear modes arising from the linear eigenvectors with total energy concentrated in the second harmonic bifurcate with finite nonzero Manley-Rowe characteristic. Moreover, in the latter case there can exist two physically distinct families bifurcating from the same linear state. These findings were at first quantified by the perturbative formal expansions which are shown to acquire different forms for the two above-mentioned situations. Then we confirmed the analytical predictions via numerical computations of the full nonlinear system, determining its nonlinear modes. We have addressed several representative sets of the system parameters and numerically computed continuous families of nonlinear modes as functions of the propagation constant.

Further, we have numerically examined the stability of the identified families. Generally, the stability was found to have rather complex properties but some gross features could still be discerned such as the systematic robustness of the modes that emerged from the linear solutions. The dynamics also features differences from the cubic case, such as the fact that the lossy waveguide does not typically appear to have a vanishing amplitude (when growth occurs on the gain side).

Finally, there are numerous directions that one can consider for future study. On the one hand, one can address simple extensions of the present dimer, such as the case with competition between the signs of γ_1 and γ_2 with gain in the first harmonic but loss in the second (or vice versa). In the way of extensions to models with more degrees of freedom, one can envision chains of such dimers at the lattice level (whereby discrete solitary waves and their properties can be considered) or even continuum extensions of the dimer in transverse continuous directions. In that case, the dimer considered herein would constitute the limit of homogeneous solutions along such transverse directions. Some of these possibilities are currently under investigation and will be reported in future presentations.

ACKNOWLEDGMENTS

The work of D.A.Z. and V.V.K. was supported by FCT (Portugal) through the Grants No. PTDC/FIS-OPT/1918/2012 and No. PEst-OE/FIS/UI0618/2011. P.G.K. gratefully acknowledges support from the US NSF under Grants No. CMMI-1000337 and No. DMS-1312856, from the US AFOSR under Grant No. FA9550-12-1-332, and from the Binational Science Foundation under Grant No. 2010239.

[1] C. M. Bender and S. Boettcher, Phys. Rev. Lett. **80**, 5243 (1998); C. M. Bender, S. Boettcher, and P. N. Meisinger, J. Math. Phys. **40**, 2201 (1999).

[2] C. M. Bender, Rep. Prog. Phys. **70**, 947 (2007).

[3] A. Ruschhaupt, F. Delgado, and J. G. Muga, J. Phys. A **38**, L171 (2005).

[4] M. Kulishov, J. Laniel, N. Bélanger, J. Azaña, and D. Plant, Opt. Express **13**, 3068 (2005).

[5] R. El-Ganainy, K. G. Makris, D. N. Christodoulides, and Z. H. Musslimani, Opt. Lett. **32**, 2632 (2007).

[6] A. Guo, G. J. Salamo, D. Duchesne, R. Morandotti, M. Volatier-Ravat, V. Aimez, G. A. Siviloglou, and D. N. Christodoulides, Phys. Rev. Lett. **103**, 093902 (2009).

[7] C. E. Rüter, K. G. Makris, R. El-Ganainy, D. N. Christodoulides, M. Segev, and D. Kip, Nat. Phys. **6**, 192 (2010).

[8] L. Feng, M. Ayache, J. Huang, Y.-L. Xu, M.-H. Lu, Y.-F. Chen, Y. Fainman, and A. Scherer, Science **333**, 729 (2011).

[9] A. Regensburger, C. Bersch, M.-A. Miri, G. Onishchukov, D. N. Christodoulides, and U. Peschel, Nature (London) **488**, 167 (2012).

[10] Z. H. Musslimani, K. G. Makris, R. El-Ganainy, and D. N. Christodoulides, Phys. Rev. Lett. **100**, 030402 (2008).

[11] H. Ramezani, T. Kottos, R. El-Ganainy, and D. N. Christodoulides, Phys. Rev. A **82**, 043803 (2010).

[12] A. A. Sukhorukov, Z. Xu, and Yu. S. Kivshar, Phys. Rev. A **82**, 043818 (2010).

[13] F. Kh. Abdullaev, V. V. Konotop, M. Ögren, and M. P. Sørensen, Opt. Lett. **36**, 4566 (2011).

[14] R. Driben and B. A. Malomed, Opt. Lett. **36**, 4323 (2011); Europhys. Lett. **96**, 51001 (2011); N. V. Alexeeva,

I. V. Barashenkov, A. A. Sukhorukov, and Yu. S. Kivshar, Phys. Rev. A **85**, 063837 (2012).
[15] Yu. V. Bludov, V. V. Konotop, and B. A. Malomed, Phys. Rev. A **87**, 013816 (2013).
[16] I. V. Barashenkov, S. V. Suchkov, A. A. Sukhorukov, S. V. Dmitriev, and Yu. S. Kivshar, Phys. Rev. A **86**, 053809 (2012).
[17] Y. V. Bludov, R. Driben, V. V. Konotop, and B. A. Malomed, J. Opt. **15**, 064010 (2013).
[18] S. V. Dmitriev, S. V. Suchkov, A. A. Sukhorukov, and Yu. S. Kivshar, Phys. Rev. A **84**, 013833 (2011).
[19] J. D'Ambroise, P. G. Kevrekidis, and S. Lepri, J. Phys. A **45**, 444012 (2012); Chaos **23**, 023109 (2013).
[20] D. Leykam, V. V. Konotop, and A. S. Desyatnikov, Opt. Lett. **38**, 371 (2013).
[21] K. Li and P. G. Kevrekidis, Phys. Rev. E **83**, 066608 (2011).
[22] K. Li, P. G. Kevrekidis, B. A. Malomed, and U. Günther, J. Phys. A **44**, 444021 (2012).
[23] D. A. Zezyulin and V. V. Konotop, Phys. Rev. Lett. **108**, 213906 (2012).
[24] K. Li, D. A. Zezyulin, V. V. Konotop, and P. G. Kevrekidis, Phys. Rev. A **87**, 033812 (2013).
[25] A. A. Sukhorukov, S. V. Dmitriev, and Yu. S. Kivshar, Opt. Lett. **37**, 2148 (2012); S. V. Suchkov, B. A. Malomed, S. V. Dmitriev, and Yu. S. Kivshar, Phys. Rev. E **84**, 046609 (2011).
[26] V. V. Konotop, D. E. Pelinovsky, and D. A. Zezyulin, Europhys. Lett. **100**, 56006 (2012).
[27] P. G. Kevrekidis, D. E. Pelinovsky, and D. Y. Tyugin, SIAM J. Appl. Dyn. Syst. **12**, 1210 (2013); J. Phys. A **46**, 365201 (2013).
[28] I. V. Barashenkov, L. Baker, and N. V. Alexeeva, Phys. Rev. A **87**, 033819 (2013).
[29] D. A. Zezyulin and V. V. Konotop, J. Phys. A **46**, 415301 (2013).
[30] A. V. Buryak, P. Di Trapani, D. V. Skryabin, and S. Trillo, Phys. Rep. **370**, 63 (2002).
[31] R. Schiek, Opt. Quantum Electron. **26**, 415 (1994).
[32] R. Schiek, Y. Baek, G. Krijnen, G. I. Stegeman, I. Baumann, and W. Sohler, Opt. Lett. **21**, 940 (1996).
[33] G. Assanto, A. Laureti-Palma, C. Sibilia, and M. Bertolotti, Opt. Commun. **110**, 599 (1994).
[34] W. C. K. Mak, B. A. Malomed, and P. L. Chu, Phys. Rev. E **55**, 6134 (1997); **57**, 1092 (1998); Opt. Commun. **154**, 145 (1998).
[35] T. Peschel, U. Peschel, and F. Lederer, Phys. Rev. E **57**, 1127 (1998).
[36] P. D. Miller and O. Bang, Phys. Rev. E **57**, 6038 (1998).
[37] S. A. Darmanyan, A. Kobyakov, and F. Lederer, Phys. Rev. E **57**, 2344 (1998).
[38] T. Pertsch, U. Peschel, and F. Lederer, Opt. Lett. **28**, 102 (2003).
[39] R. Iwanow, R. Schiek, G. I. Stegeman, T. Pertsch, F. Lederer, Y. Min, and W. Sohler, Phys. Rev. Lett. **93**, 113902 (2004).
[40] H. Susanto, R. L. Horne, N. Whitaker, and P. G. Kevrekidis, Phys. Rev. A **77**, 033805 (2008).
[41] B. A. Malomed, P. G. Kevrekidis, D. J. Frantzeskakis, H. E. Nistazakis, and A. N. Yannacopoulos, Phys. Rev. E **65**, 056606 (2002).
[42] H. Susanto, P. G. Kevrekidis, R. Carretero-González, B. A. Malomed, and D. J. Frantzeskakis, Phys. Rev. Lett. **99**, 214103 (2007).
[43] F. C. Moreira, F. Kh. Abdullaev, V. V. Konotop, and A. V. Yulin, Phys. Rev. A **86**, 053815 (2012).
[44] F. C. Moreira, V. V. Konotop, and B. A. Malomed, Phys. Rev. A **87**, 013832 (2013).